Journal of Solid State Chemistry 184 (2011) 2661–2667

Contents lists available at ScienceDirect

Journal of Solid State Chemistry

journal homepage: www.elsevier.com/locate/jssc

Mid-infrared spectroscopic study of crystallization of cubic spinel phase from metakaolin

Petr Ptáček*, František Šoukal, Tomáš Opravil, Magdaléna Nosková, Jaromír Havlica, Jiří Brandštetr

Brno University of Technology, Faculty of Chemistry, Centre for Materials Research CZ.1.05/2.1.00/01.0012, Purkyňova 464/118, Brno CZ-61200, Czech Republic

ARTICLE INFO

Article history:
Received 6 May 2011
Received in revised form
11 July 2011
Accepted 23 July 2011
Available online 3 August 2011

Keywords:
Metakaolin
Thermal conversion
γ-Al_2O_3
Al–Si spinel
Infrared spectroscopy

ABSTRACT

The structural changes during thermal conversion of metakaolinite into cubic spinel phase that was in literature considered as Al–Si spinel or γ-Al_2O_3 were investigated by mid-infrared spectroscopy (FT-IR) and differential scanning calorimetry (DSC) using medium ordered kaolin with high content of kaolinite. Spectrum features were studied in the mid-infrared region from 4000 to 400 cm^{-1} as function of fractional conversion that resulted from DSC experiments. The increasing contends of Al–O bonds in the octahedral position (AlO_6) was observed during thermal transformation. The high ratio of antisymmetric stretching of $\equiv$Si–O–Al$\equiv$ and $\equiv$Si–O–Si$\equiv$ bands and bands belonging to stretching of $=$Al–O bonds in the (AlO_4) tetrahedra and (AlO_6) octahedra decreases exponentially with fractional conversion. The antisymmetric stretching band of $\equiv$Si–O–Si$\equiv$ bond in the (SiO_4) tetrahedra becomes more expressive due to formation of amorphous SiO_2 phase.

1. Introduction

The clays are important and useful raw materials in ceramics, chemical and food industry. Industrial meanings and utilization of important clay minerals, such as kaolinite, smectites, palygorskite and sepiolite were itemized in works [1,2]. Kaolinite ($Al_2Si_2O_5(OH)_4$ or $Al_2O_3 \cdot 2SiO_2 \cdot 2H_2O$ by oxide formula) is the main mineral component of kaolin. From mineralogical point of view kaolin phyllosilicate belongs to the kaolinite and serpentine group.

Structure of mineral is composed of two sheets of tetrahedrons $[SiO_4]^{4-}$ ("T" layer) and octahedrons $[AlO_3(OH)_3]^{6-}$ ("O" layer or gibbsite sheet) interconnected by apical oxygen atom [1].

Thermal transformation of kaolinite in to thermodynamic stable phases (Eqs. (1)–(4)), i.e. mullite ($Al_2[Al_{2+2x}Si_{2-2x}\square_x]O_{10-x}$, where $\square_x$ gives the number of oxygen vacancies per unit cell and value of x is ranging from 0.17 to 0.59, or oxide formula $3Al_2O_3 \cdot 2SiO_2$) and cristobalite (c-SiO_2), has been studied by a number of authors using different methods [3–6,16]. The temperature sequences of thermal transformation of kaolinite into different products are illustrated by the following equations:

$$Al_2O_3 \cdot 2SiO \cdot 2H_2O \xrightarrow{400-700\,^{\circ}C} Al_2O_3 \cdot 2SiO\ (\text{metakaolinite}) + 2H_2O \quad (1)$$

$$\text{Metakaolinite} \xrightarrow{980\,^{\circ}C} \begin{cases} \text{Al-Si spinel phase (20–30 wt\%)} \\ \text{Mullit (trace of weakly crystalline)} \\ \text{Aluminosilicate phase (amorphous, 30–40 wt\%)} \\ SiO_2\ \text{(amorphous, } \sim 36\,\text{wt\%)} \end{cases} \quad (2)$$

or

$$2\,(Al_2O_3 \cdot 2SiO_2) \longrightarrow 2Al_2O_3 \cdot 3SiO_2 + SiO_2(\text{amorphous})$$

$$3(2Al_2O_3 \cdot 3SiO_2) \xrightarrow{>1100\,^{\circ}C} 2\,(3Al_2O_3 \cdot 2SiO_2) + 5\ SiO_2(\text{amorphous}) \quad (3)$$

$$SiO_2(\text{amorphous}) \xrightarrow{>1150\,^{\circ}C} c\text{-}SiO_2(\text{cristobalite}) \quad (4)$$

The occurring processes and qualities of products (Eqs. (1)–(4)) are strongly affected by properties of original kaolinite such as particle shape and particle size distribution, degree of crystallization and order of kaolinite structure, adsorbed and substituted ions, presence and amount of impurities or accessory minerals of kaolinite and conditions of thermal treatment [7–10]. Well ordered kaolinite is transformed into less reactive metakolinite [11]. Mechanical [12,13] and ultrasound treatment [14] of well-ordered kaolinite increase structural disorder, delamination of kaolinite structure as well as reduction of the particle size.

Mullite is the only thermodynamically stable compound that is formed in the alumina–silica system under atmospheric pressure. Therefore, considerable interests were devoted to synthesis of mullite [15–19]. The sol–gel process [20,21], precipitation method [22–24], molten salt method [25,26], spray pyrolysis

* Corresponding author.
E-mail address: ptacek@fch.vutbr.cz (P. Ptáček).

0022-4596/$ - see front matter © 2011 Elsevier Inc. All rights reserved.
doi:10.1016/j.jssc.2011.07.038

[27] and other sophisticated methods [28–31] were applied in the fore-mentioned literature dedicated to synthesize mullite. Formed intermediates, temperature interval of synthesis, crystallinity and product homogeneity depend on the applied method, precursors, agent of mineralization and heating rate [32–34]. In the case that raw material contains high amount of calcium or magnesium carbonates admixtures such as calcite ($CaCO_3$) or dolomite ($CaMg(CO_3)_2$), the gehlenite ($Ca_2Al(AlSi)O_7$), anorthite ($CaAl_2Si_2O_8$) and akermanite ($Ca_2MgSi_2O_7$) were formed [35,36].

Much attention was paid to transformation of transitional cubic phase of the metakaolinite to mullite as well. Although, the formation of γ-Al_2O_3 with the fcc (face-centered cubic) oxygen structure is originally supposed [37] and this phase was also identified in other works [38,39]. The material is often described to have defective spinel structure, where Al ions is occupying both octahedral and tetrahedral sites [40]. Thermal decomposition of matekaoline into oxide phases (Al_2O_3, SiO_2) seems to be not favorable from the thermodynamic point of view. Furthermore if the formed cubic phase is γ-Al_2O_3, it should be transformed into α-Al_2O_3, nevertheless mullite was form [37]. Many of published works [3,16,41,42] support the formation Al–Si spinel ($Si_3Al_4O_{12}$ or $2Al_2O_3 \cdot 3SiO_2$) that is one of intermediates of mullite rising during thermal treatment of kaolinite (Eq. (2)).

Although there is great support that Al–Si spinel phase is probably formed during treatment of kaolinite, the universal consensus still is not be reached [37]. Pask and Tomsia [43] are claimed that occurred processes are affected by heating rate and formation of spinel and pseudotetragonal mullite are competitive reactions. On the other hand, the γ-Al_2O_3 as well as other modifications of Al_2O_3 is the common intermediates during thermal synthesis of mullite using different salt and alkoxide precursors or aluminum hydroxides (gibbsite, bayerite) and oxide–hydroxides (boehmite, diaspore) [6,26,39,44–48].

The infrared spectroscopy may provide useful information about phase sequence and mechanism of formation of mullite due to sensitivity of this method towards tetrahedrally and octahedrally coordinated aluminum atoms as well as amorphous silica phase. The process is connected with changes of parameters of the absorption bands located in the spectral region from 1200 to 400 cm^{-1} [6,40,49,50].

The present paper aims to investigate the mechanism and kinetics of cubic phase formation occurring (under) during thermal

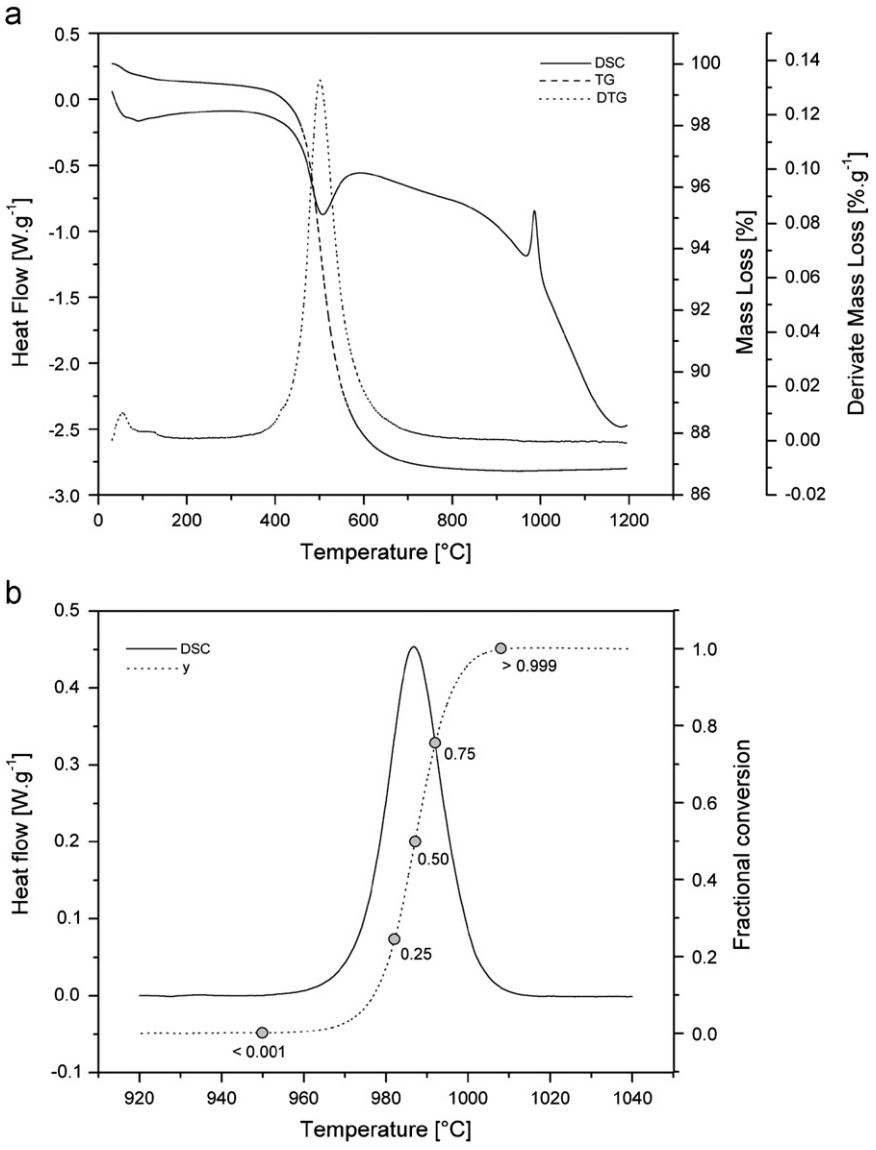

Fig. 1. DSC-TGA plot of kaolin (a) and detail of baseline corrected Al–Si spinel peak with fractional conversion curve (b). The position of samples used for FT-IR assessments is highlighted.

treatment of kaolin. The mid-infrared spectroscopy was used to study the structural changes of samples heated to different temperatures within metakaolinite to Al–Si spinel transition interval so that different degree of conversion was reached. The changes in the spectra were studied as the function of fractional conversion.

2. Experimental

2.1. Sample characterization

Washed kaolin Sedlec Ia from the region Carlsbad (Czech Republic) produced by the company Sedlecký kaolin a.s. was used for the study of thermal decomposition of kaolinite. This high quality kaolin, originally mined in open-cast mine near village Sedlec, is commercially available since 1892 and it is often allowed to be the world's standard. The content of kaolinite guaranteed by producer is higher than 90% wt. with equivalent grain diameter median in the range 1.2–1.4 μm. The main impurities are mica group minerals and quartz. The colorant oxides content – hematite (α-Fe_2O_3) and tetragonal TiO_2 (rutile) – is lower than 0.85 and 0.2% wt., respectively. The initial state, properties and chemical composition of applied kaolin is described in work [51].

2.2. Preparation and analysis of the samples

Thermal treatment of analyzed samples was proceeded directly in the TG-DTA analyzer (Q600, Thermal Instruments) which works in DSC mode in order to improve the comparison between experimental data collected by individual experimental techniques and estimated fractional conversion or degree of conversion (y) of the samples heated at given temperature.

Fractional conversion (please refer to Fig. 1(b)) for crystallization of spinel phase was estimated from DSC results using ratio:

$$y = \frac{I_T}{I_P} \tag{5}$$

where I_T and I_P are areas of peak integrated from the beginning to temperature T and total area under the DSC peak, respectively.

The temperatures for which value of spinel phase fractional conversion has reached $\geq$0.1%, 25%, 50%, 75% and $\geq$99.9% (Fig. 1(b)) were evaluated from TG-DSC experiment over temperature region from 22 to 1200 °C using heating rate (Θ) 10 °C min^{-1}. The individual samples were heated under the equal conditions to temperatures related to the certain value of y and next fast cooled the temperature bellow formation interval of spinel phase (100 °C min^{-1}). All the heating experiments are three times repeated to obtain the average results without outlier values.

Structural changes, which take place during formation of spinel phase from thermal treated kaolinite was investigated by Fourier transform infrared spectroscopy (FT-IR) using FT-IR analyzer Nicolet iS10 (Thermo Scientific). The KBr pellets technique was used for measurements of spectra. Sample was carefully weighted and mixed with dry KBr in the mass ratio 1:100 and pellets with weight 120 mg were hand pressed from the mixture. That enables to keep comparable optical length of prepared pellets.

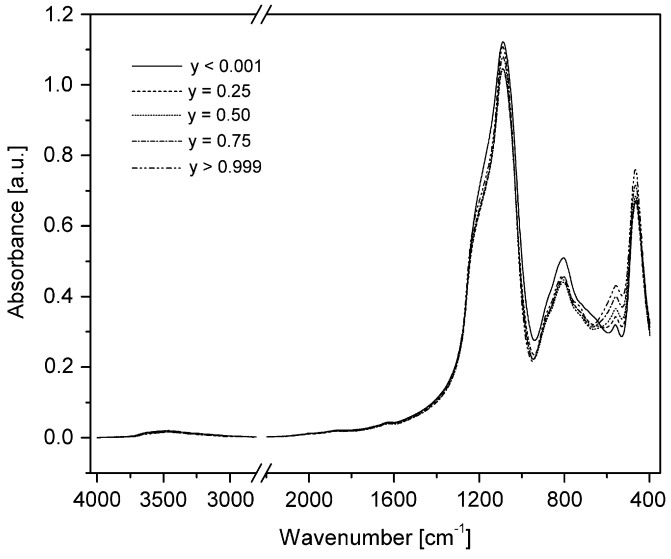

Fig. 2. Baseline corrected average infrared spectra of samples treated to temperature interval of formation of Al–Si spinel.

3. Results and discussion

3.1. Thermal analysis

The typical DSC-TGA pattern of thermal decomposition of kaolin is shown in Fig. 1(a). The mass of the sample is reduced by evaporation of adsorbed water and dehydroxylation about 0.55% and 12.59%, respectively.

The dehydroxylation is followed by combustion of organic admixtures that are present always in clay compounds in various degrees. This exothermic process of organic admixture combustion is masked by endothermic dehydroxylation on DTA curves, but it is evidenced by a small effect on left side shoulder of DTG peak [52]. It must be pointed out that the position of this effect depends on the composition of organic matter and its amount. Both the processes interact because water vapor formed by dehydroxylation slow down combustion of organic admixtures. On other hand water formed by combustion of organic compounds increases partial pressure of water vapor and that slow down dehydroxylation process.

Table 1
Changes of spectra connected with formation of spinel phase.

y	T (°C)	ν_{max} (cm^{-1})/Absorption intensity (a.u.)			
<0.001	950	1089.27/0.947	804.04/0.404	560.97/0.231	464.16/0.561
0.25	982	1090.03/0.989	803.89/0.398	559.96/0.285	465.68/0.631
0.50	987	1089.66/1.063	804.94/0.431	558.00/0.364	466.20/0.711
0.75	991	1089.60/1.048	805.54/0.422	558.63/0.383	466.70/0.723
>0.999	1008	1090.50/1.036	807.38/0.410	558.24/0.390	466.46/0.721
Band assignment		ν_{as}(≡Si–O–Si≡) ν_{as}(≡Si–O–Al≡)[a]	ν(≡Al–O) in (AlO_4) tetrahedron	ν(≡Al–O) in (AlO_6) octahedron	δ(≡Si–O) in (SiO_4) tetrahedron
References		[6,32,49,50]	[49,50]	[49,50]	[49,50]

[a] Shoulder of band.

Exothermic transformation of metakaolinite into spinel phase (Eq. (2)) takes place at 986 °C under applied heating rate 10 °C min^{-1}. The temperatures of onset and outset of peak are 974 °C and 1001 °C, respectively. The peak was subtracted, integrated and obtained data were used to calculate the fractional conversion (Fig. 1(b)) according to Eq. (5).

3.2. Infrared spectroscopy

The FT-IR spectra measured for samples heated to temperature that is corresponding to given value of fractional conversion are shown in Fig. 2.

The main features in the spectra of prepared samples are listed in Table 1. Formation of spinel phase is connected with the changes in the position, shape and intensity of bands in the spectra.

In existing literatures [6,32,49,50,53], bands that are located in the spectral region from 1400 to 850 cm^{-1} are assigned to symmetric and antisymmetric stretching modes of ≡Si–O–Si≡ and ≡Si–O–Al═ bridge, respectively. The presence of tetrahedrally (AlO_4) and octahedrally (AlO_6) coordinated ═Al–O bonds provides stretching mode bands within interval ranged from 850 to 750 cm^{-1} and from 750 to 500 cm^{-1}, respectively. The deformation modes of (SiO_4) and (AlO_6) are located at wavenumber below 500 and 440 cm^{-1}, respectively.

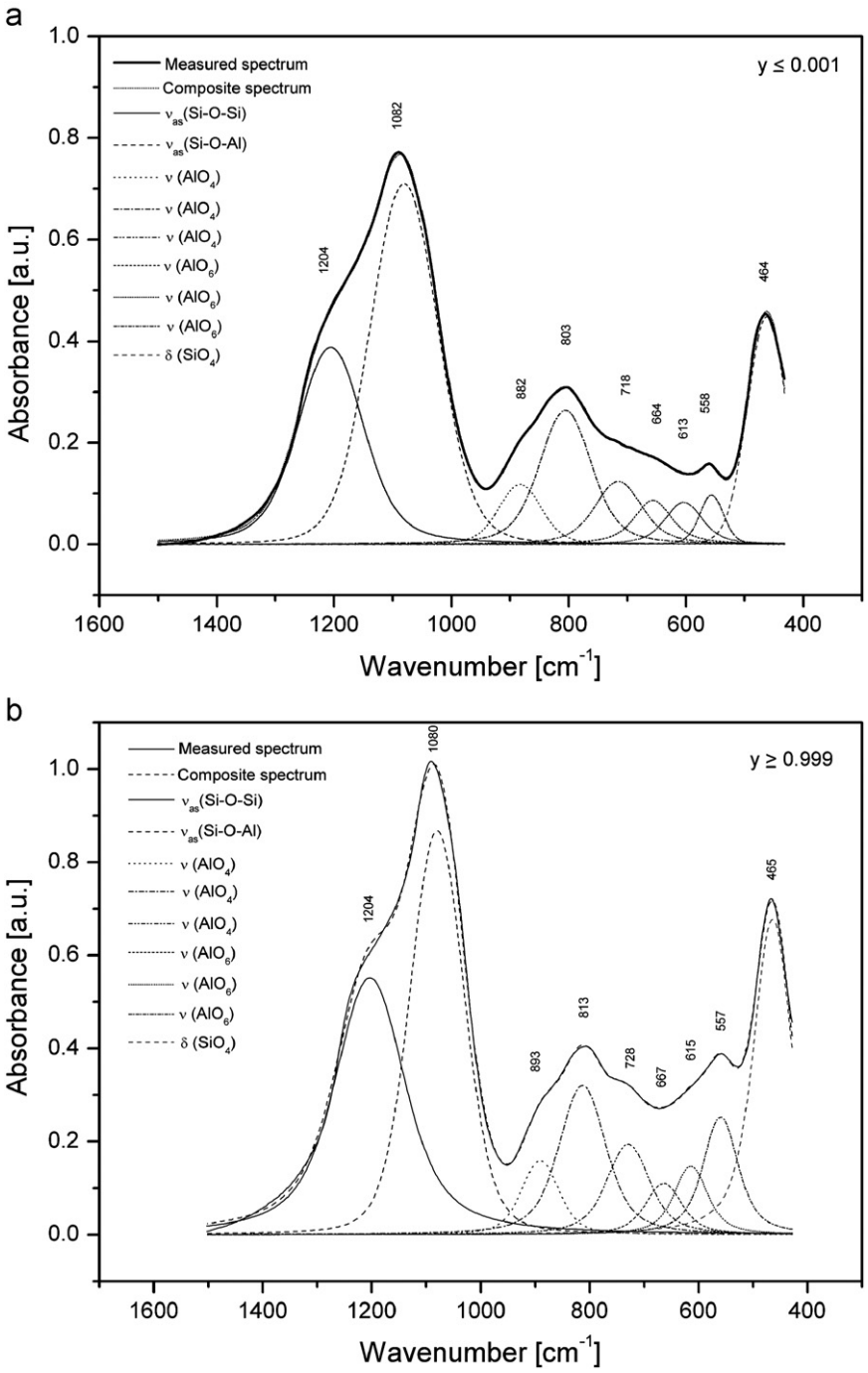

Fig. 3. Approximation of inert structure of spectrum by Voigt functions for samples $y \leq 0.001$ and $y \geq 0.999$.

Table 2
Parameters of fitted bands in infrared spectra of samples treated to temperature interval of formation of spinel phase.

Band assignment	Parameter of band	Fractional conversion of sample				
		< 0.001	**0.25**	**0.50**	**0.75**	**> 0.999**
≡Si–O–Si≡(antisymmetric stretching)	ν_{max} (cm^{-1})	1204.9	1204.4	1206.5	1204.1	1202.6
	$w_{1/2}$	68.9	63.4	57.2	63.0	64.2
	Height (a.u.)	0.457	0.486	0.528	0.541	0.562
≡Si–O–Al=(antisymmetric stretching)	ν_{max} (cm^{-1})	1080.4	1080.7	1081.1	1080.4	1080.2
	$w_{1/2}$	121.2	107.1	107.9	103.0	103.3
	Height (a.u.)	0.842	0.881	0.935	0.930	0.918
=Al–O in (AlO_4) tetrahedral (stretching modes)	ν_{max} (cm^{-1})	882.7	886.1	888.2	889.9	892.0
	$w_{1/2}$	71.1	69.1	68.5	71.7	66.2
	Height (a.u.)	0.149	0.145	0.159	0.160	0.154
	ν_{max} (cm^{-1})	805.2	806.0	807.6	809.1	812.0
	$w_{1/2}$	78.7	79.6	79.3	79.4	79.7
	Height (a.u.)	0.323	0.321	0.347	0.342	0.317
	ν_{max} (cm^{-1})	719.0	719.3	721.4	721.95	724.3
	$w_{1/2}$	56.5	57.4	58.1	58.1	59.8
	Height (a.u.)	0.143	0.168	0.190	0.227	0.201
=Al–O in (AlO_6) octahedral (bending and stretching modes of AlO_4 and AlO_6)	ν_{max} (cm^{-1})	667.1	661.9	659.7	658.9	658.9
	$w_{1/2}$	51.4	51.8	52.8	53.8	53.5
	Height (a.u.)	0.113	0.117	0.122	0.146	0.114
	ν_{max} (cm^{-1})	612.3	606.5	604.5	604.2	602.9
	$w_{1/2}$	60.8	58.8	59.7	64.2	64.0
	Height (a.u.)	0.138	0.154	0.186	0.199	0.201
	ν_{max} (cm^{-1})	558.6	556.5	554.3	553.7	553.6
	$w_{1/2}$	42.7	45.8	50.7	53.0	52.1
	Height (a.u.)	0.117	0.153	0.197	0.211	0.202
≡Si–O in (SiO_4) tetrahedral (bending)	ν_{max} (cm^{-1})	462.8	463.2	464.3	465.2	464.8
	$w_{1/2}$	63.2	63.7	60.1	57.6	57.8
	Height (a.u.)	0.560	0.643	0.678	0.704	0.692

The wavenumber of maximum absorption intensity (ν_{max}) of ν_{as}(≡Si–O–Al=) mode and its absorption intensity has increased with fractional conversion. The shoulder of band, which is assigned to ν_{as}(≡Si–O–Si≡) of (SiO_4) tetrahedra becomes more expressive during formation of spinel phase. The absorption intensity and ν_{max} of deformation mode of ≡Si–O bonds in (SiO_4) tetrahedra is rising as well. The rising absorption intensity of ≡Si–O–Si≡ linkages indicates increasing amount of amorphous silica that is formed according to Eq. (2).

The contrary evolution of the features of bands belonging to (AlO_4) tetrahedra and (AlO_6) octahedra with temperature were observed. While wavenumber of maximum absorption intensity is increasing for stretching of =Al–O bond in the tetrahedral coordination, the value of ν_{max} is decreasing for octahedral coordination. Absorption intensity of $\nu(AlO_6)$ increases, but $\nu(AlO_4)$ shows maximum at fractional conversion 0.5 of treated sample.

The shape of bands listed in Table 1 indicates that spectrum (Fig. 2) contains other unresolved features. In order to obtain more detailed results about the evolution of the absorption profile during formation of spinel phase was region from 1500 to 400 cm^{-1} fitted by the Voight function. The typical results of fitting procedure are shown in Fig. 3.

The fitted spectrum show that the broad band of =Al–O stretching mode in the (AlO_4) tetrahedron contains two substructures with maximum absorption intensity at around 888 ± 5 and 723 ± 3 cm^{-1}. The other two wide bands in fitted spectrum (665 ± 3 and 610 ± 3 cm^{-1}) are placed within energy region of =Al–O bending and stretching motion of both (AlO_4) and (AlO_6) unit [53].

The parameters of absorption bands determined for all samples are listed in the Table 2. Obtained data prove observed increasing intensity of antisymmetric stretching of ≡Si–O–Si≡ (siloxane) bridge as the results of formation of amorphous silica according to Eq. (2) and minimum intensity of ν_{as}(≡Si–O–Al=) mode for $y = 0.5$. The amorphous state of SiO_2 bring higher variation of structure, i.e. higher variation of energy of ≡Si–O–Si≡ bonds, and that leads to observed increasing of band half-width.

The height ratio of bands which belong to ≡Si–O–Al= and ≡Si–O–Si≡ antisymmetric stretching (R_{as}) is decreasing with fractional conversion exponentially (Fig. 4(a)). This enables to estimate the stage of spinel formation from infrared spectrum of thermal treated sample according to following formula:

$$R_{as} = 1.91 - 0.06 \exp\left[-\frac{y}{0.67}\right] \quad (6)$$

This indicates the increase of amount of ≡Si–O–Si≡ to ≡Si–O–Al= bonds during transformation of metakaoline into spinel.

The height ratio of the most expressive stretching bands of =Al–O in the (AlO_4) tetrahedra and (AlO_6) octahedra (R_s) with time decreases exponentially (Fig. 4 (b)). The obtained dependence respects well the equation:

$$R_s = 1.51 + 1.26 \exp\left[-\frac{y}{0.33}\right] \quad (7)$$

The amount of tetrahedrally coordinated sites is decreasing to certain limit value that is, according to Eq. (7), equal to 1.51. The presence of both (AlO_4) and octahedrally sites (AlO_6) indicates that metakaolinite is converted into spinel. Both the dependences in Fig. 4 show fractional conversion equal to 0.5, where reached value of R_{as} and R_s ratio is 1.77.

4. Conclusion

The relationship between band features and fractional conversion is more expressive than that between temperature and fractional conversion. Because apart from temperature, the fractional

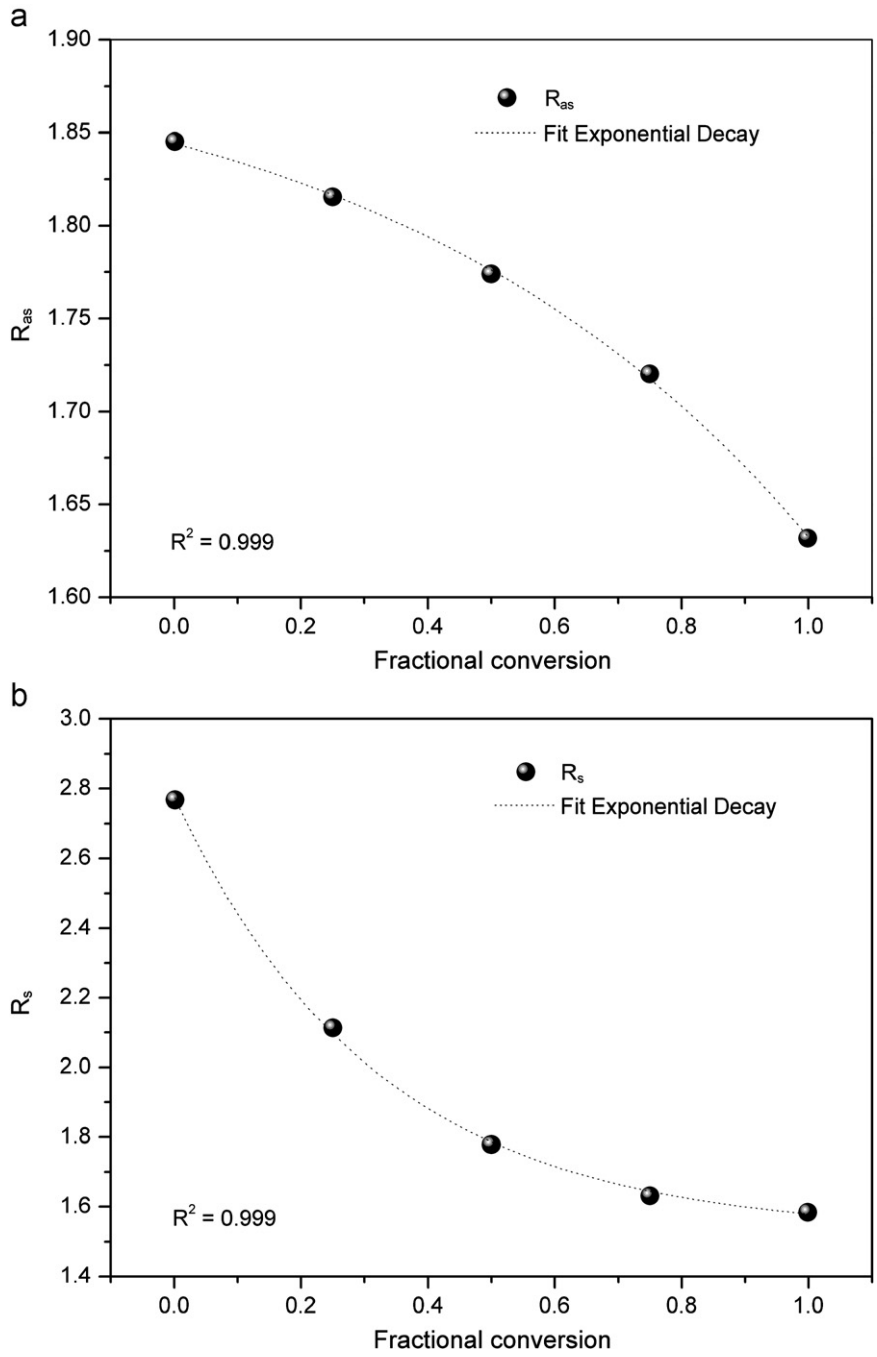

Fig. 4. The dependence of ≡Si–O–Al≡ to ≡Si–O–Si≡ (R_{as}) and (AlO_4) to (AlO_6) ratio (R_s) on fractional conversion.

conversion depends also on many factors such as sample mass, particle size distribution, heating rate, etc. that may not always guarantee the reproducibility of the experimental measurements.

The spectrum features indicates increasing content of octahedrally coordinated Al atoms during thermal transformation of metakaoline into cubic spinel phase. The Al ions occupy both tetrahedral and octahedral sites and that is indicating formation the defective spinel structure of γ-Al_2O_3.

The intensity ratio of bands belonging to stretching of (AlO_4) tetrahedra and (AlO_6) octahedra decreases exponentially with fractional conversion. The intensity of antisymmetric stretching band of ≡Si–O–Si≡ bond in the (SiO_4) tetrahedra increases due to formation of silica phase. The intensity ratio of antisymmetric stretching of ≡Si–O–Al≡ and ≡Si–O–Si≡ shows increase of ≡Si–O–Si≡ bonds during transformation of metakaoline into spinel structure.

Acknowledgments

This paper is a result of the research project supported by the Ministry of Education, Youth and Sports No. 2B08024 and project no. CZ.1.05/2.1.00/01.0012 "Centres for Materials Research at FCH BUT" supported by operational program Research and Development for Innovations.

References

[1] J. Konta, Applied Clay Science 10 (1995) 275–335.
[2] H.H. Murray, Applied Clay Science 17 (2000) 207–221.
[3] V. Balek, M. Murat, Thermochimica Acta 282–283 (1996) 385–397.
[4] W.D. Keller, Developments in Sedimentology 27 (1979) 581–590.
[5] A.K. Chakraborty, Thermochimica Acta 398 (2003) 203–209.

[6] C.H. Rüscher, G. Schrader, M. Götte, Journal of the European Ceramic Society 16 (1996) 169–175.
[7] K. Heide, M. Földvari, Thermochimica Acta 446 (2006) 106–112.
[8] J. Dubois, M. Murat, A. Amroune, X. Carbonneau, R. Gardon, Applied Clay Science 10 (1995) 187–198.
[9] J. Temuujin, K. Okada, K.J.D. MacKenzie, Ts. Jadambaa, Journal of the European Ceramic Society 19 (1999) 105–112.
[10] Ch. Bich, J. Ambroise, J. Péra, Applied Clay Science 44 (2009) 194–200.
[11] G. Kakali, T. Perraki, S. Tsivilis, E. Badogiannis, Applied Clay Science 20 (2001) 73–80.
[12] C. Vizcayno, R. Castelló, I. Ranz, B. Calvo, Thermochimica Acta 428 (2005) 173–183.
[13] E. Horváth, R.L. Frost, É. Makó, J. Kristóf, T. Cseh, Thermochimica Acta 404 (2003) 227–234.
[14] F. Franco, L.A. Pérez-Maqueda, J.L. Pérez-Rodríguez, Journal of Colloid and Interface Science 274 (2004) 107–117.
[15] M. Romero, J. Martín-Márquez, J Ma. Rincón, Journal of the European Ceramic Society 26 (2006) 1647–1652.
[16] Y.-F. Chen, M.-Ch Wang, M.-H. Hon, Journal of the European Ceramic Society 24 (2004) 2389–2397.
[17] B. Bagchi, S. Das, A. Bhattacharya, R. Basu, P. Nandy, Applied Clay Science 47 (2010) 409–413.
[18] O. Castelein, B. Soulestin, J.P. Bonnet, P. Blanchart, Ceramics International 27 (2001) 517–522.
[19] C.Y. Chen, W.H. Tuan, Ceramics International 26 (2000) 715–720.
[20] X. Chen, L. Gu, Journal of Materials Processing Technology 209 (2009) 3991–3998.
[21] Y. Zhang, Y. Ding, J. Gao, J. Yang, Journal of the European Ceramic Society 29 (2009) 1101–1107.
[22] S. Satoshi, C. Contreras, H. Juárez, A. Aguilera, J. Serrato, International Journal of Inorganic Materials 3 (2001) 625–632.
[23] S.S. Sueyoshi, C.A.C. Soto, Journal of the European Ceramic Society 18 (1998) 1145–1152.
[24] S. Wang, X.-Q. Shen, H.-Ch Yao, Z.-J. Li, Ceramics International 36 (2010) 761–766.
[25] P. Zhang, J. Liu, H. Du, Z. Li, S. Li, S. Li, R. Xu, Journal of Alloys and Compounds 491 (2010) 447–451.
[26] L. Saadi, R Moussa, A. Samdi, A. Mosset, Journal of the European Ceramic Society 19 (1999) 517–520.
[27] Dj. Janackovic, V. Jokanovic, Lj. Kostic-Gvozdenovic, D. Uskokovic, Nanostructured Materials 10 (1998) 341–348.
[28] T. Michalet, M. Parlier, F. Beclin, R. Duclos, J. Crampon, Journal of the European Ceramic Society 22 (2002) 143–152.
[29] T.Y. Yang, H.B. Ji, S.Y. Yoon, B.K. Kim, H.C. Park, Conservation and Recycling 54 (2010) 816–820.
[30] Z. Chen, L. Zhang, L. Cheng, P. Xiao, G. Duo, Journal of Materials Processing Technology 166 (2005) 183–187.
[31] A. Esharghawi, C. Penot, F. Nardou, Ceramics International 36 (2010) 231–239.
[32] J. Li, H. Lin, J. Li, J. Wu, Journal of the European Ceramic Society 29 (2009) 2929–2936.
[33] G.M. Anilkumar, P. Mukundan, A.D. Damodaran, K.G.K. Warrier, Materials Letters 33 (1997) 117–122.
[34] L.B. Kong, Y.Z. Chen, T.S. Zhang, J. Ma, F. Boey, H. Huang, Ceramics International 30 (2004) 1319–1323.
[35] K. Traoré, T.S. Kabré, P. Blanchart, Ceramics International 29 (2003) 377–383.
[36] T. Toya, Y. Tamura, Y. Kameshima, K. Okada, Ceramics International 30 (2004) 983–989.
[37] I.M. Low, R.R. McPherson, Journal of Materials Science Letters 7 (1988) 1196–1198.
[38] H. Schneider, K. Okada, J.A. Pask, Mullite and Mullite Ceramics, John Wiley, Chichester, 1994.
[39] A. kr. Chakraborty, S. Das, Ceramics International 29 (2003) 27–33.
[40] M.-H. Lee, Ch.-F. Cheng, V. Heine, J. Klinowski, Chemical Physics Letters 265 (1997) 673–676.
[41] P. Ptáček, F. Šoukal, T. Opravil, M. Nosková, J. Havlica, J. Brandštetr, Journal of Solid State Chemistry 183 (2010) 2565–2569.
[42] W. Brindley, M. Nakahira, Journal of the American Ceramic Society 42 (1959) 319–324.
[43] J.A. Pask, A.P. Tomsia, Journal of the American Ceramic Society 74 (1991) 2367–2373.
[44] K. Okada, J. Kaneda, Y. Kameshima, A. Yasumori, T. Takei, Materials Letters 57 (2003) 3155–3159.
[45] H. Ivankovic, E. Tkalcec, R. Nass, H. Schmidt, Journal of the European Ceramic Society 23 (2003) 283–292.
[46] E. Tkalcec, H. Ivankovic, R. Nass, H. Schmidt, Journal of the European Ceramic Society 23 (2003) 1465–1475.
[47] H. Schneider, D. Voll, B. Saruhan, M. Schmücker, T. Schaller, A. Sebald, Journal of the European Ceramic Society 13 (1994) 441–448.
[48] H. Schneider, B. Saruhan, D. Voll, L. Merwin, A. Sebald, Journal of the European Ceramic Society 11 (1993) 87–94.
[49] S. Shoval, M. Boudeulle, S. Yariv, O. Lapides, G. Panczer, Optical Materials 16 (2001) 319–327.
[50] P. Padmaja, G.M. Anilkumar, P. Mukundan, G. Aruldhas, K.G.K. Warrier, International Journal of Inorganic Materials 3 (2001) 693–698.
[51] P. Ptáček, D. Kubátová, J. Havlica, J. Brandštetr, F. Šoukal, T. Opravil, Isothermal kinetic analysis of the thermal decomposition of kaolinite: the thermogravimetric study, Thermochimica Acta 501 (2010) 24–29.
[52] P. Ptáček, F. Šoukal, T. Opravil, M. Nosková, J. Havlica, J. Brandštetr, The non-isothermal kinetics analysis of the thermal decomposition of kaolinite by effluent gas analysis technique, Powder Technology 203 (2010) 272–276.
[53] L. Favaro, A. Boumaza, P. Roy, J. Lédion, G. Sattonnay, J.B. Brubach, A.M. Huntz, R. Tétot, Journal of Solid State Chemistry 183 (2010) 901–908.